



# Novel pH-sensitive triptolide-loaded micelles: a potential approach to increase anti-tumor activity of the diterpenoid epoxide

Zhimeng Lu · Kun Yan · Chunlei Liu ·  
Jiapeng Wang · Guiping Yu · Hao Zhang

Received: 15 December 2023 / Accepted: 2 March 2024  
© The Author(s) 2024

**Abstract** *Tripterygium wilfordii* Hook F, a traditional medicine in China has bioactive but toxic triptolide (TP, a diterpenoid triepoxide) as its main active constituents. The applications of TP are hampered by its prominent toxicity and low solubility in water. In this study, a safe pH-sensitive material [methoxy polyethylene glycol (mPEG)- adipic dihydrazide (ADH)] was synthesized and loaded with TP to form pH-sensitive polymeric micelles, thereby improving the safety and solubility of TP, as well as providing a theoretical basis for the wide application of TP. The mPEG-ADH/TP micelles were characterized by a series of indicators [namely entrapment efficiency (EE), critical micellar concentration (CMC), electrokinetic potential, stability, polydispersed index (PDI), and particle size]. Also, we ascertained the in vitro

release of TP from mPEG-ADH/TP micelles along with pharmacokinetic investigations in vivo. Besides, we evaluated the cytotoxicity of mPEG-ADH/TP micelles against A549 cells, HCT116 cells, and HaCat cells and further conducted in vivo toxicity studies in rats. The TP-loaded mPEG-ADH micelles had smaller sized particles (48.3 nm), excellent PDI (0.142), stable property and higher EE (89.87%). Importantly, the TP in the mPEG-ADH/TP micelles was almost completely released at acidic pH (pH 5.0), while the drug was released slowly and sparingly at physiological pH (pH 7.4). The results suggest the release of TP from mPEG-ADH/TP micelles was sensitive to pH, which could facilitate targeting of the drug into intra-cellularly low pH endosomes and lysosomes as well as enhance cytotoxicity in cancer tissues. Moreover, mPEG-ADH/TP micelles exhibited excellent proliferation inhibition on tumor cells. In addition, the liver injury of rats in the 1 mg/kg dose of mPEG-ADH/TP micelles group was significantly reduced by Hematoxylin–eosin (HE) staining. Taken together, mPEG-ADH/TP micelles could act as a promising alternative to enhance the efficacy of oncologic treatments.

Zhimeng Lu and Kun Yan contributed equally to this work.

Z. Lu · K. Yan · G. Yu (✉)  
Department of Thoracic and Cardiovascular Surgery,  
Jiangyin Clinical College Affiliated to Xuzhou Medical  
University, Jiangyin 214400, Jiangsu, China  
e-mail: xiaoyuer97103@163.com

C. Liu · J. Wang  
Department of Pharmaceutics, School of Pharmacy,  
Jiangsu University, Zhenjiang City 212013, Jiangsu, China

H. Zhang (✉)  
Department of Thoracic Surgery, Affiliated Hospital  
of Xuzhou Medical University, Xuzhou 221004, Jiangsu,  
China  
e-mail: haozhang\_xz@163.com

**Keywords** Triptolide · mPEG-ADH · pH-sensitive ·  
Micelles · Anti-tumor · Nanobiomedicine

## Introduction

*Tripterygium wilfordii* Hook F (TWHF), also known as *Lei Gong Teng*, is a traditional Chinese herb that has been widely used for centuries in China [1]. Several types of bioactive substances such as alkaloids, diterpenes [triptolide (TP), triptonide and triptolide], glycosides, lignans, sesquiterpenes, and triterpenes (wilforlide A, pristimerin and celastrol) have been isolated and identified from TWHF [2, 3]. In particular, the most active constituent of TWHF with potential applications is TP. Hence, numerous pre-clinical and clinical works have shown the pharmacological potentials of TP. Notable among them include anti-inflammation, immunosuppression [4] (particularly during prolonged graft survival from organ transplantation), and anti-tumor (e.g. cancers of the pancreas [5], lung [6], osteogenic sarcoma [7], and lymphatic system [8]). Apart from inhibiting the growth of tumors and metastasis along with directly inducing the death of cancerous cells, TP also increases the anti-tumor activity of chemotherapeutic and cytotoxic drugs. Despite the multiple pharmacological activities offered, clinical use of TP remains limited due to its systemic toxicity [9], narrow therapeutic windows, and poor solubility [10]. Therefore, scientists have made an attempt to minimize adverse effects and increase the therapeutic index of TP in cancer treatment. In this regard, some nano-carriers of TP have been developed, namely, nanoparticles targeting CD44 [11] and HER2 [12], chlorin e6-supra-molecular nanosystem [13], self-micellar solid dispersion [14], PEGylated and casein self-assembled nanoparticles [15, 16], and exosomes [17]. In spite of the prospects of the abovementioned nanosystems in the clinical applications of TP, the ultimate aim of decreasing the systemic toxicities and increasing bioavailability of the drug in cancer tissues has still not been completely achieved. Thus, other alternative nano-preparations are needed for the abovementioned purposes.

In chemotherapy, scientists have broadly utilized various types of nanoparticles as systems of drug delivery, namely polymeric micelles, dendritic polymers, inorganic molecules, and liposomes [18]. Scientists have developed much interest in polymeric micelles, inter alia, and other nano-platforms in tumor treatment. Of note, some of these micellar systems have undergone clinical studies [19]. In aqueous surroundings, spherically core-shell structures like

micelles are formed via self-assembling of amphiphilic copolymers. Usually, lipophilic drugs are incorporated into hydrophobic core of the micelle, while stability and prolongation of drug circulation time in blood are provided by a micellar hydrophilic shell [20, 21]. The micellar platforms are biocompatible and have the potential to entrap all-inclusive drugs with the ability to accumulate preferentially in cancer tissues through enhanced permeability-and-retention (EPR) effects [22].

Despite these advantages of conventional polymeric micelles, their drug release is slow and incomplete, thereby resulting in insufficient concentrations to cause death of cancer tissues. Additionally, drugs can be released prematurely which may cause harmful effects [23]. In recent times, micelles that are sensitive to stimuli have been widely developed in the pursuit of better therapeutic efficacy and reduced toxicity [24–26]. The advantages of stimuli-responsive micelles include superior stability, improved tumor accumulation, desirable endocytosis, and better drug-release capabilities [27, 28]. In cancer treatment, sustained drug release systems like micelles that are sensitive to pH have shown great potential among the entire stimuli-sensitive micellar platforms. At physiological pH, micelles that are sensitive to pH remain stable but at acidic pH, they become structurally unstable. Since there is a difference between the pH of healthy tissue (pH 7.4) and that of the intra-cellular surroundings of cancer tissues (pH 6.5), particularly in lysosomes and endosomes (pH 4.5–5.5), where pH-sensitive micelles can release encapsulated drugs at specific tumor sites [23].

Herein, a pH-sensitive material [methoxy polyethylene glycol (mPEG)- adipic dihydrazide (ADH)] was synthesized and its safety was investigated. Afterwards, the TP-loaded mPEG-ADH micelles (mPEG-ADH/TP micelles) were prepared and characterized by a series of indicators [namely entrapment efficiency (EE), critical micellar concentration (CMC), electrokinetic potential, stability, polydispersed index (PDI), and micellar size of particles]. To assess the stability of the micelles, we evaluated the physicochemical features for 30 days. Subsequently, we carried out in vitro drug release and pharmacokinetic studies of the mPEG-ADH/TP micelles, while 3-(4,5-dimethyl-thiazol-2-yl)-2,5-diphenyl-tetra-zolium bromide (MTT) and flow apoptotic assays were employed to evaluate the cytotoxicity of mPEG-ADH/

TP micelles against A549 cells. Putatively, mPEG-ADH/TP micelles could serve as a targeted treatment option for cancer.

## Materials and methods

### Materials

The TP was acquired from Macklin (Shanghai, China). ADH, methoxy polyethylene glycol carboxyl (mPEG-COOH, MW5000), 1-(3-Dimethylaminopropyl)-3-ethylcarbodiimide hydrochloride (EDC), 1-Hydroxybenzotriazole (HOBt), and triethylamine (Et<sub>3</sub>N) were purchased from Aladdin (Shanghai, China). Dimethylsulfoxide (DMSO) and dichloromethane (DCM) were obtained from TEDIA (OH, USA). All other chemicals were of analytical grade. Thermo Fisher Scientific (NH, USA) supplied RPMI-1640 medium, Hematoxylin–eosin (HE) staining kit, and Dulbecco-Modified Eagle medium (DMEM).

### Synthesis of mPEG-ADH

The ADH (70 mg, 0.4 mmol) was dissolved in DMSO (5 ml), while the reaction was stirred under the protection of N<sub>2</sub> for 1 h until the product changed from a transparent solid to turbidity. Later on, we dissolved mPEG-COOH (200 mg, 0.04 mmol) in DCM, EDC (9.2 mg, 0.048 mmol), and HOBt (6.4 mg, 0.048 mmol), while Et<sub>3</sub>N (22 μL, 0.16 mmol) was gradually added to activate the carboxylic acid via stirring for 4 h under N<sub>2</sub>. The mixture was then added in dropwise fashion to the ADH solution using a syringe for 1 day followed by DCM removal. After the reaction, the mixture was transferred into a dialysis membrane and dialyzed against distilled water for 2 days, wherein the mPEG-ADH was obtained through rotavap (80 °C, 100 rpm). The chemical structure of mPEG-COOH and mPEG-ADH were confirmed using <sup>1</sup>H NMR spectrum in CDCl<sub>3</sub> or DMSO-d<sub>6</sub>.

### Safety assessment of mPEG-ADH

The MTT assay was employed to ascertain in vitro cytotoxicity of mPEG-ADH with murine kidney podocytes (MPC-5). Briefly, MPC-5 cells were seeded in 96-well plates (1 × 10<sup>4</sup> cells/well) before 24 h of incubation at 37 °C in atmospheric 5%-CO<sub>2</sub>

before treatment. Later, we exposed the cells to a series of concentrations (5, 10, 25, 50, 100, 250, 500, and 1000 μg/ml) of mPEG-ADH for 48 h. After incubation, we added DMSO (100 μl) to the cells prior to 10 min of incubation under the same aforementioned conditions. The absorbance was measured by an automatic microplate reader (Bio-Tek, USA) at 490 nm. The following equation was employed to calculate the viability of cells: cell viability (%) = OD<sub>sample</sub> / OD<sub>control</sub> × 100%.

### Establishment of high-performance liquid chromatography (HPLC) analysis method

In vitro TP concentration was measured with the HPLC system comprised of a CTO-20A UV differential detector, a CTO-20AC column oven, a LC-20AC quaternary pump, and a SIL-20AC automatic sampler (Shimadzu-Japan) on a reverse ODS-C18 column (5 μm, 4.6 × 150 mm; Waters-USA). We performed the separation chromatographically at a 1.0 ml/min flow rate under the condition of 219 nm detection wavelength and 30 °C column temperature. The mobile phase was acetonitrile/0.1% phosphoric acid–water solution (55/45, v/v), while the sample injection volume was 20 μL. The standard curve of TP was  $Y = 32.798 \times C + 45.976$  (linear range, 1–100 μg/mL;  $R^2 = 0.9993$ ), wherein  $Y$  denoted peak areas and  $C$  depicted concentration of TP. Also, in vivo TP concentration was also determined as mentioned above. Of note, we chose the internal standard (IS) to be diosmetin (10 μg/mL). Through the HPLC system, we separated peaks of TP and IS in plasma successfully with no endogenous molecules interfering the process.

### Preparation of mPEG-ADH/TP micelles

The TP-loaded mPEG-ADH micelles were prepared using a thin-film dispersion method [29]. Later, we transferred the TP and mPEG-ADH in methanol to a boiling flask before ultrasonication at 30 kHz for 30 min to ensure complete dissolution to obtain a mixed solution. In order to obtain a thin film, we removed the organic solvent with rotavap (45 °C, 60 rpm/min). Afterwards, we hydrated the film with sterile water and vortexed the solution for 30 min at 37 °C to form mPEG-ADH/TP micelles. The optimization of mPEG-ADH/TP micelles was conducted by adjusting the ratios of mPEG-ADH and

TP (15:1, 12:1, 10:1, 8:1, 6:1, 4:1). The particle sizes, PDI, and EE were selected as evaluation indicators of the optimized formulation.

#### Characterization of mPEG-ADH/TP micelles

Particle size/electrokinetic potential analyzer (90Plus PALS, Brookhaven, USA) was utilized to determine micellar particle size, electrokinetic potential, and PDI using the dynamic light scattering technique. The morphology of micelles was observed using a transmission electron microscopy (TEM, JEM-2100, Electronics Corporation, Japan). The samples for morphological observation with TEM were prepared as follows; we dispersed aliquot of micelles onto a copper-grid before air dried at ambient temperature. Later, we stained the samples with a solution (2%) of phosphotungstate. After the appropriate drying process, we placed the copper-grid under TEM for morphological observation.

The EE (%) was measured by Sephadex gel chromatography. The column was filled with 50 g of dextran gel G-50. Next, the micelles (1 mg/mL) were added to the chromatographic column and eluted with purified water. An eluted portion of purified water was collected every 10 ml for HPLC analysis and the amount of encapsulated TP was calculated. When TP was not detected in the eluted portion of purified water, 0.2% NaCl solution was added and the eluted portion was taken as the unencapsulated TP. The EE (%) was calculated as follows:  $EE (\%) = \frac{\text{the quantity of TP encapsulated in micelles}}{\text{the quantity of initial amount of TP}} \times 100\%$ .

#### Stability of mPEG-ADH/TP micelles

The stability of mPEG-ADH/TP micelles was evaluated at 4 °C and 25 °C for 30 days, wherein the micelles were prepared as described earlier in this report and stored in an airtight glass vial without hydration [30]. Afterwards, the particle sizes, PDI and EE were measured on days 1, 15, and 30.

#### Measurement of CMC

A fluorescent probe (pyrene) was used to estimate the CMC value of mPEG-ADH/TP micelles via the spectrofluorimetric technique as described in previous work [30].

In brief, 40  $\mu$ L pyrene stock solution (0.06 mol/L in tetrahydrofuran) was added to each 10 mL brown tube and placed in an open fume hood for 12 h to evaporate the organic solvent. To attain the final concentration of pyrene (0.0006 mol/L), we added the micellar solution at different concentrations (1, 2.5, 5, 10, 20, 50, 100, 200, and 400  $\mu$ g/mL) into each tube. Afterwards, we carried out 30 min of ultrasonication of the tubes before keeping them for 12 h at ambient temperature. The fluorescent spectrophotometric technique was utilized to measure fluorescent intensity with an excitation wavelength of 338 nm and emission spectrum ranging 300 to 500 nm. Later, we recorded the intensity ratio [ $I_{373}$ ]/ $I_{383}$ ] prior to the analysis and computation of CMC.

#### pH-sensitive detection

The mPEG-ADH/TP micelles were diluted to about 200  $\mu$ g/mL with a buffer solution of pH 5.0 and shaken for about 10 min. Later on, we placed aliquot of the diluted micelles on copper-grid before staining the samples with solution (2%) phosphotungstate and ultimately examined and photographed with TEM.

The dialysis method was employed to test the in vitro release pattern of TP from mPEG-ADH/TP micelles. Concisely, we filled the dialysis tubing (at molecular weight-cutoff of 3000 Da) with solutions (0.5 mg) of TP and mPEG-ADH/TP micelles. Later on, we completely tied the bags at both ends and carried out the dialysis in 100 ml of four different media (namely distilled water, pH 7.0; phosphate-buffered saline, PBS, pH 7.4; PBS, pH 6.8; PBS, pH 5.0) at 37 °C and 100 rpm. At predetermined time intervals (0.083, 0.25, 0.5, 1, 2, 4, 6, 8, 12, 24, and 48 h), we sampled aliquot (1 ml, each) of the above media and replenished appropriately with freshly prepared medium at equal volume. Samples were centrifuged at 10,000 rpm for 10 min, followed by analysis with HPLC. The cumulative release of TP that was loaded into micelles was calculated as ratio to total TP with the following equations:  $\text{the cumulative release } \% = \frac{\text{cumulative amount of TP in the release medium}}{\text{total amount of TP in mPEG-ADH/TP micelles}} \times 100\%$ .

#### Cellular uptake study

The uptake of mPEG-ADH/TP micelles by human lung adenocarcinoma cells (A549) was carried out as described elsewhere with some modifications [31,

32]. The cells were cultured in a DMEM growth medium that comprised of streptomycin (100 mg/mL), fetal-bovine serum (FBS, 10%, v/v), and penicillin (100 IU/mL). Culturing of the cells was carried out under the same conditions described in the above section (*safety assessment of mPEG-ADH*). FITC was used instead of TP, wherein it was loaded into micelles through the preparation method described above. Later, we added mPEG-ADH/FITC micelles to the cells before incubation for 1, 2, 4, 8, 12, and 24 h. Subsequently, the cells were fixed with 4% paraformaldehyde for 20 min. After that, we washed the cells four times with pH 7.4 PBS. Next, nuclear staining was completed with DAPI, while the cells were incubated at 37 °C for 20 min. Anti-fluorescence burst sealing solution was dropped onto the samples using a 1 mL pipette. The cells were observed with a fluorescence inverted microscope, wherein green color indicated FITC spectrum, and DAPI-labelled nuclei was depicted by blue light. A preliminary investigation of the uptake mechanism of mPEG-ADH/TP micelles was carried out by preincubating the cells with cytochalasin D (Cyt D, 10 µM, an inhibitor of endocytosis) before subsequent incubation with of mPEG-ADH/TP micelles for 1, 2, 3, 4, 5, 6, 12, and 24 h. Afterwards, we captured images using a confocal laser scanning microscope (LSM780 NLO, Zeiss, Germany). We performed the entire experiments thrice and recorded the measurements in triplicates.

#### Pharmacokinetics study

Male Sprague–Dawley (SD) rats (weighing  $200 \pm 20$  g) were purchased from the laboratory animal research center of Jiangsu University. Apart from unrestricted access to water and food, the rats were also kept in cages that were maintained at appropriate environmental conditions (30–70% humidity and 25 °C temperature) with a cycle of 12 h darkness and light.

The SD rats intravenously received the same doses (1 mg/kg) of TP and mPEG-ADH/TP at their tails, accordingly. After that, whole blood was harvested at 0.083 h, 0.25 h, 0.5 h, 0.75 h, 1 h, 1.5 h, 2 h, 3 h, 4 h, 6 h, 8 h, 10 h, 12 h, and 24 h. Then, the whole blood was subjected to 10 min of centrifugation at 3700 rpm to obtain plasma. Afterward, we diluted plasma (200 µL) containing IS in methanol.

Later on, the samples were detected with the HPLC system. The peak areas of TP and IS were recorded, and concentrations of TP were calculated by substituting into the in vivo standard curve. The BAPP software (Nanjing, China) was relied on to calculate the main parameters of pharmacokinetics namely maximum drug concentrations (drug concentrations ( $C_{\max}$ )), times of achieving  $C_{\max}$  ( $T_{\max}$ ), half-life of TP ( $T_{1/2}$ ), mean-residence time (MRT), and area under the curve of concentration curve in plasma ( $AUC_{0-\infty}$ ).

#### In vitro anti-tumor activity

##### *Inhibition rate detection*

To evaluate the potential of TP, mPEG-ADH/TP micelles and mPEG-ADH to inhibit the growth of A549, HCT116, and HaCat cell lines, we seeded the cells onto 96 well plates before 24 h of culturing. Afterwards, we substituted the cultured medium with FBS-free medium that contained TP, mPEG-ADH/TP micelles, and mPEG-ADH at a series of TP concentrations of 0.1, 0.5, 1, 5, 10, 20, and 50 µg/mL for another 48 h. The control was the cells that were incubated with an FBS-free medium. At the specified time, we added MTT solution (20 µL) into the plates. After incubation for 4 h, we added DMSO (100 µL) before 10 min of incubation. An automatic microplate reader was utilized to measure the absorbance at 490 nm.

##### *Apoptotic rate and flow cytometric analysis*

Briefly, we incubated the A549 cells for 48 h with TP and mPEG-ADH/TP micelles (0.1, 0.5, 1, 5, 10, 20, and 50 µg/mL). The treated cells were collected and washed. The addition of the dye was performed under light-avoidance conditions. No dye was added to the non-stained group, while we added PI or Annexin V (5 µL) to the single-stained batch, each (5 µL) of PI and Annexin V was added to the double-stained batch. After incubation for 15 min at room temperature and under protection from light, 300 µL of 1×binding buffer was added and mixed well, before cell suspensions were transferred to flow tubes (5 mL). The cells were detected on a flow cytometer within 1 h. The analysis of profiles was accomplished with FlowJo software.

### Calculation of median lethal dose (LD50)

Rats were injected with 0.1, 0.2, 0.4, 0.8, 1.0, 1.5, 2.0, and 4.0 mg/kg of TP ( $n = 10$ ) via tail vein injection, and the mortality rate was calculated as median lethal dose median lethal dose (LD50).

### Hematoxylin–eosin (HE) staining

HE pathological sections of the liver of 1.0 and 2.0 mg/kg rats in TP and mPEG-ADH/TP micelles groups were analyzed. After the rats were killed, liver tissues were collected, embedded in paraffin, and made into sections. The tissues were then stained with hematoxylin and eosin and observed under a photoelectric microscope. The specific procedure of the experiment followed the manufacturer's protocol.

### Statistical analysis

Herein, GraphPad prism software was utilized for the statistical analysis. After we have expressed the data with mean, standard deviation (SD), and confidence interval (95%), we applied Student's *t*-test to ascertain the difference within the experimented groups.

Statistically, acceptance of significant differences was agreed at  $p < 0.05$ .

## Results

### Characterization of mPEG-ADH

The synthesis pathway of mPEG-ADH is shown in Fig. 1a. The structure of mPEG-COOH, mPEG-ADH, and ADH were confirmed with  $^1\text{H}$  NMR spectrum (Fig. 1b–d). The  $^1\text{H}$  NMR spectrum of synthetic product displayed two typical peaks at 1.5 ppm and 2.2 ppm of ADH. The result demonstrated the mPEG-ADH has been synthesized successfully. It could be found in the  $^1\text{H}$  NMR spectrum of ADH (Fig. 1d) that ADH has a hydrogen signal between chemical shifts 1–2, while mPEG-COOH has no hydrogen signal in this interval, and the product ADH-mPEG-COOH also has a hydrogen signal between chemical shifts 1–2, which fully indicated that ADH-mPEG-COOH has been prepared.

When we evaluated the cytotoxicity of mPEG-ADH against MPC-5 cells with MTT assay, we observed that mPEG-ADH demonstrated negligible cytotoxicity to MPC-5 cells after 48 h of incubation,

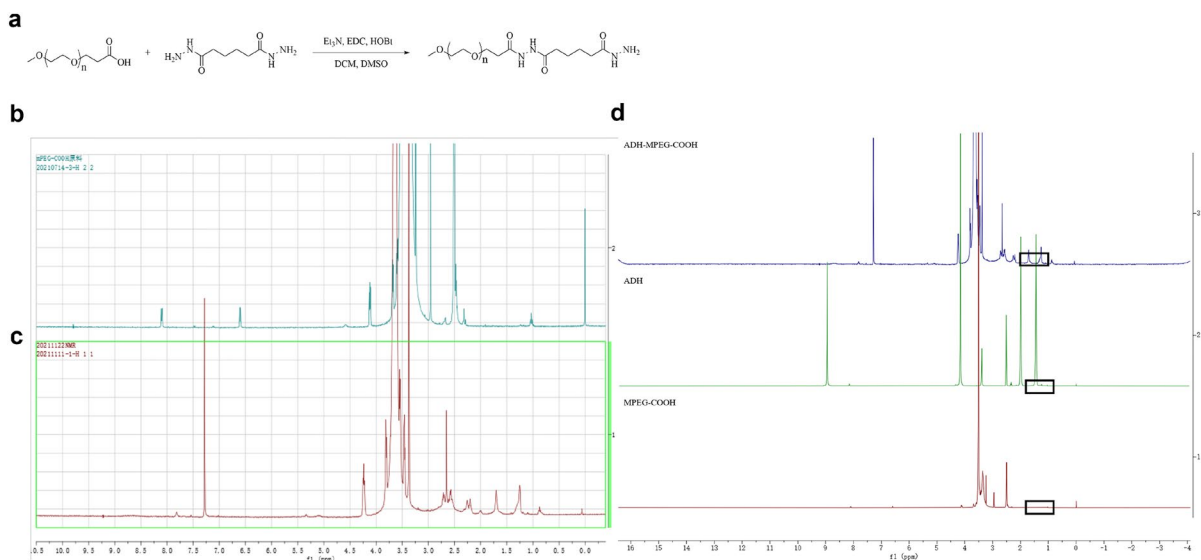


**Fig. 1** Synthesis of methoxy polyethylene glycol- adipic dihydrazide (mPEG-ADH). **a** mPEG-ADH synthesis roadmap. **b**  $^1\text{H}$  NMR spectrum of mPEG-COOH in DMSO- $d_6$ . **c** mPEG-

ADH in CDCl<sub>3</sub>. **d**  $^1\text{H}$  NMR spectrum of ADH-mPEG-COOH, ADH, and mPEG-COOH in DMSO- $d_6$

wherein the viability of the cell remained over 85% until concentration of 500  $\mu\text{g}/\text{mL}$  was attained (Fig. 2). The results indicated a good safety profile for the pH-sensitive material (mPEG-ADH).

### HPLC analysis

The HPLC chromatogram of TP in vitro is shown in Fig. 3. The peak of TP was well separated with a retention time of 4.6 min (Fig. 3a). The HPLC chromatogram of TP and IS in vivo was shown in Fig. 3b. Peak shapes of TP and IS were good

without being interfered by that of endogenic impureness. Additionally, we observed distinct separation of the peaks of TP and IS with respective retention times of 4.6 and 16.5 min. On this basis, we chose diosmetin as appropriate IS for this study. Consequently, the established method was feasible for the detection of TP in vitro and in vivo.

### Characterization of mPEG-ADH/TP micelles

The formulation of mPEG-ADH/TP micelles was investigated by assessing particle size, PDI, and EE.

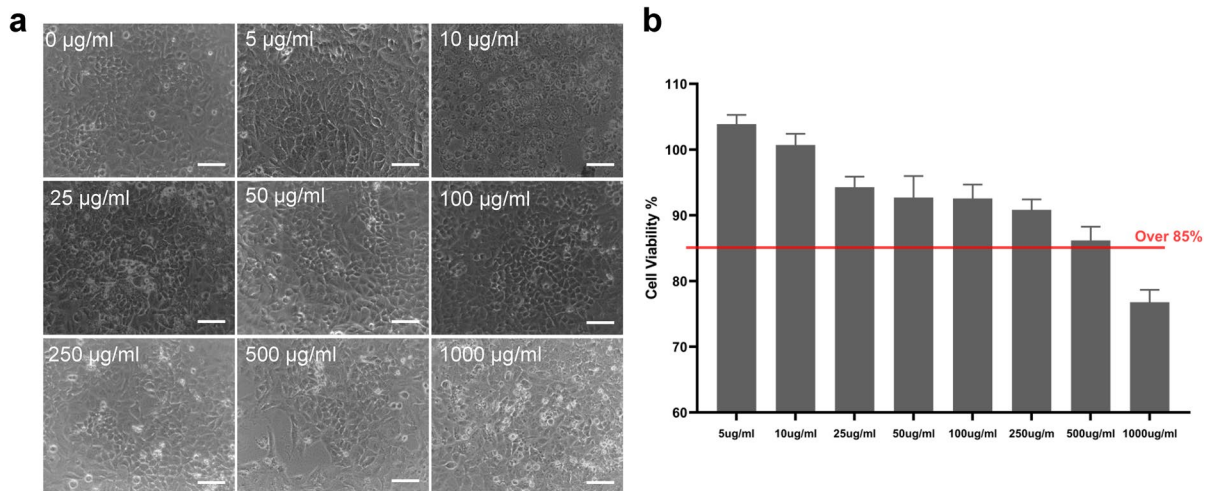


**Fig. 2** Safety profile of methoxy polyethylene glycol- adipic dihydrazide (mPEG-ADH). **a** MPC-5 cells statuses after treatment with different concentrations of mPEG-ADH materials

(Scar bar=50  $\mu\text{m}$ ). **b** Cell viability of MPC-5 cells treated with different concentrations of mPEG-ADH materials

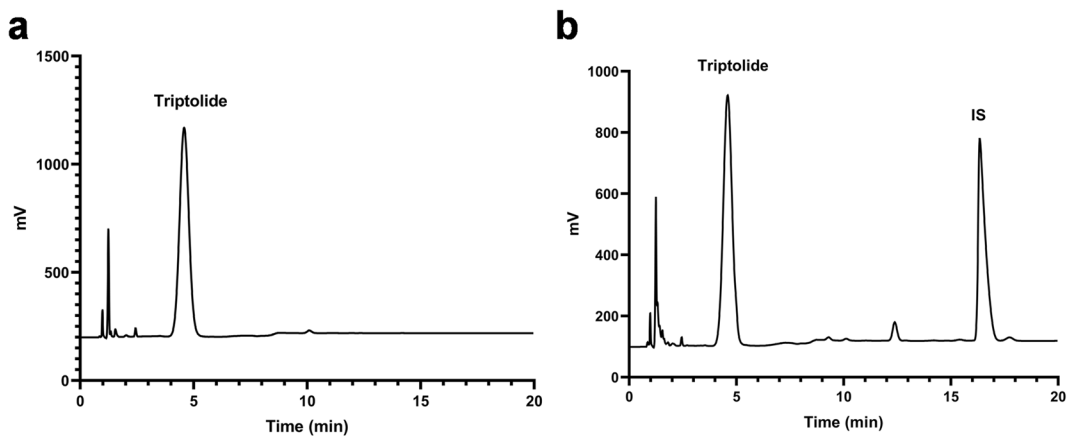


**Fig. 3** HPLC analysis in vitro and in vivo. **a** TP in vitro. **b** Blank plasma mixed with TP and IS

As shown in Table 1, the optimal ratio of mPEG-ADH to TP was 10:1. In the current work, particle size, electrokinetic potential, PDI, morphology, EE, and stability were applied to characterize the mPEG-ADH/TP micelles. Consequently, results of the particle size distribution and morphology of mPEG-ADH/

**Table 1** Three indicators (diameter, polydispersity index-PDI, entrapment efficiency-EE) for micelles of different ratio of mPEG-ADH to TP ( $n=3$ , mean  $\pm$  SD)

mPEG-ADH: TP	Diameter (nm)	PDI	EE (%)
15:1	45.1 $\pm$ 1.21	0.138 $\pm$ 0.021	65.22 $\pm$ 0.23
12:1	41.2 $\pm$ 2.01	0.139 $\pm$ 0.014	71.39 $\pm$ 0.31
10:1	48.3 $\pm$ 1.29	0.142 $\pm$ 0.011	89.87 $\pm$ 0.26
8:1	65.2 $\pm$ 2.39	0.242 $\pm$ 0.019	88.38 $\pm$ 0.34
6:1	79.2 $\pm$ 2.01	0.265 $\pm$ 0.027	92.12 $\pm$ 0.51
4:1	97.8 $\pm$ 2.83	0.271 $\pm$ 0.031	92.51 $\pm$ 0.55

TP micelles are shown in Fig. 4a and b, while a detailed stability study is summarized in Table 2. The mPEG-ADH/TP micelles showed single and narrow particle size distribution with the mean size of micellar particles being  $48.3 \pm 1.29$  nm and electrokinetic potential of  $-28.31 \pm 1.28$  mV and PDI of  $0.142 \pm 0.011$ . The estimated size confirmed that our preparation was indeed micelles since the diameter of such microstructure is below 50 nm. Further, TP was successfully incorporated into the micelles with a high EE (89.87%). This observation may be attributable to the possible interaction between the carbonyl groups of ADH and TP. To affirm the increased stability of mPEG-ADH/TP micelles, we carried out the assessment of micellar storage stableness at 4 °C and 25 °C for 30 days. In this regard, we did not observed the occurrence of any substantial alterations in EE, PDI, and particle size at days 1, 15, and 30 under the tested condition. Hence, we concluded

**Fig. 4** Characterization of methoxy polyethylene glycol- adipic dihydrazide/ triptolide (mPEG-ADH/TP) micelles. **a** The particle size distribution of mPEG-ADH/TP micelles. **b** The morphology (TEM image) of mPEG-ADH/TP micelles. **c** The intensity ratio (I373/I383) of the pyrene emission spectra versus the log concentration of TP

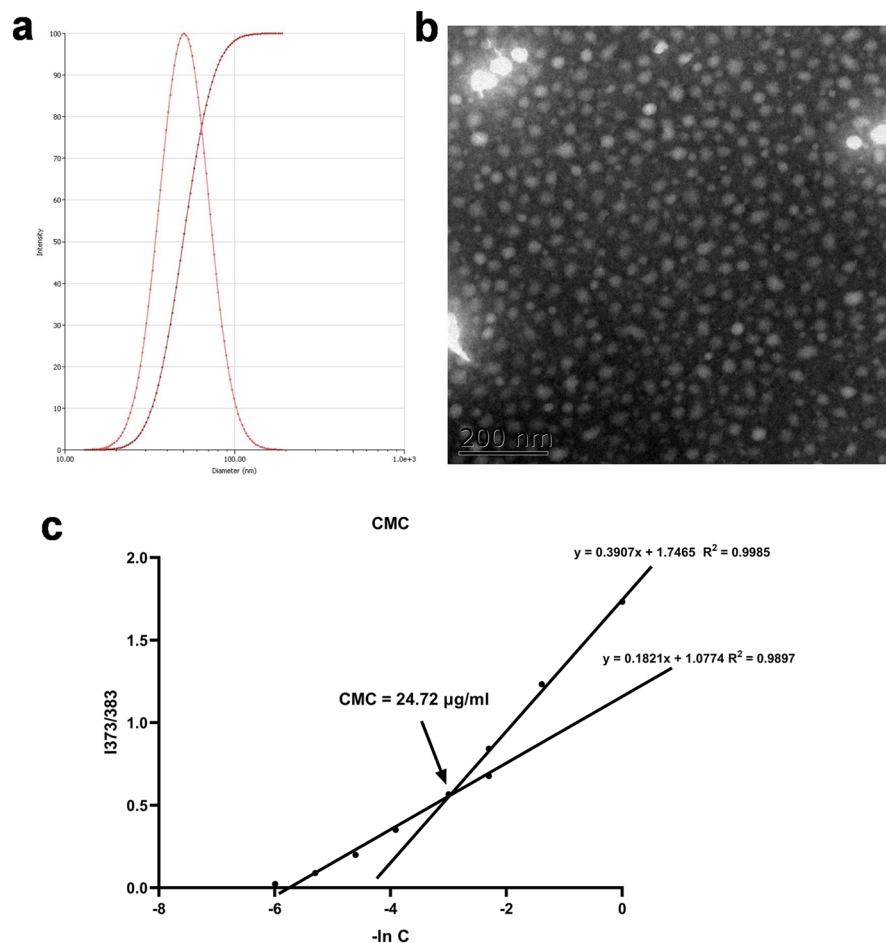




**Table 2** Stability of methoxy polyethylene glycol- adipic dihydrazide/triitolide (mPEG-ADH/TP) micelles ( $n = 3$ , mean  $\pm$  SD)

Time	4 °C			25 °C		
	Day 1	Day 15	Day 30	Day 1	Day 15	Day 30
Diameter (nm)	48.18 $\pm$ 0.29	48.78 $\pm$ 0.43	49.44 $\pm$ 0.60	48.22 $\pm$ 0.30	49.44 $\pm$ 0.33	51.15 $\pm$ 0.23
PDI	0.142 $\pm$ 0.005	0.143 $\pm$ 0.006	0.147 $\pm$ 0.005	0.143 $\pm$ 0.006	0.147 $\pm$ 0.002	0.155 $\pm$ 0.004
EE (%)	89.65 $\pm$ 0.44	88.55 $\pm$ 0.58	87.63 $\pm$ 0.46	89.67 $\pm$ 0.43	88.50 $\pm$ 0.58	86.25 $\pm$ 0.48

that mPEG-ADH/TP micelles were stable and could be stored at the tested conditions.

#### Estimation of CMC

In estimating the value of CMC of micellar solutions, the pyrene method has emerged as one of the important and sensitive methods. Through plotting of micellar concentration against fluorescent intensity, formulation scientists can estimate the CMC value. Since molecules of pyrene binds to the core of the micellar structure, it is expected that the fluorescent intensity will increase when the concentration of the micelles also increases. Hence, the intersection of two straight-line curves can be utilized to estimate CMC value. As shown in Fig. 4c, CMC was found to be 24.72  $\mu$ g/mL, which indicates micelle was formed at lower concentrations of the materials.

#### TP release profile

TEM image from Fig. 5a showed that TP was released from micelles after treatment with pH 5.0 buffer solution. The illustration in Fig. 5b depicts in vitro release trend of unencapsulated TP and mPEG-ADH/TP micelles (pH 5.0, pH 6.8, pH 7.0, and pH 7.4). In comparison to unencapsulated TP, mPEG-ADH/TP micelles exhibited a rapid release profile. Within 24 h, we discovered that the release of TP from mPEG-ADH/TP micelles was nearly 100% at acidic pH (pH 5.0), which is the closest pH to lysosomes and endosomes of tumor sites. However, the cumulative release of unencapsulated TP through the dialysis bag at pH 5.0 was up to 50% at 24 h. At other pH values (pH 6.8, pH 7.0, and pH 7.4), neither free TP nor mPEG-ADH/TP micelles fully released the drug. The observed trend may imply sustained release

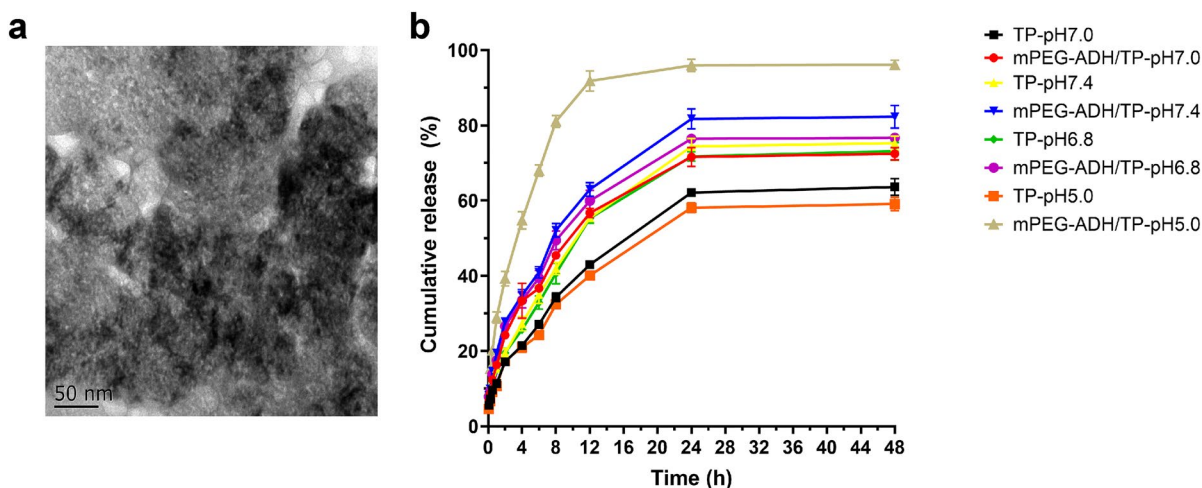


**Fig. 5** pH-sensitive assessment. **a** The morphology (TEM image) of methoxy polyethylene glycol- adipic dihydrazide/triitolide (mPEG-ADH/TP) micelles treated with pH 5.0 buffer solution. **b** The in vitro drug release behaviors of the

unencapsulated TP and mPEG-ADH/TP micelles in phosphate-buffered solution (PBS, pH 5.0), PBS (pH 6.8), water (pH 7.0), and PBS (pH 7.4)

of TP from mPEG-ADH/TP micelles at physiological pH but faster release of the drug at acidic pH.

#### Cellular uptake of mPEG-ADH/FITC micelles

Since FITC is fluorescent probe, we utilized FITC fluorescence to evaluate micellar uptake by A549 cells via fluorescence microscopic technique. The mPEG-ADH/FITC micelles were obviously internalized by the tumor cells particularly at 8 h via an unknown mechanistic pathway, which resulted in the accumulation of the drug inter-cellularly, and subsequent promotion of drug uptake. Increase in mPEG-ADH/FITC micelles uptake by the A549 cells before 8 h was dependent on time; thereafter, we observed gradual decline in uptake (Fig. 6a). In order to elucidate the particular internalization pathways of mPEG-ADH/TP micelles, we evaluated the effects of endocytosis inhibitor (i.e., Cyt D) on

the uptake of the micelles into the A459 cells. We observed that mPEG-ADH/TP micelles could be internalized into A459 cells via endocytosis since treatment of the cells with Cyt D suppressed further uptake of the micelles (Fig. 6b). Of note, Cyt D has been found to inhibit actin polymerization, macropinocytosis, and phagocytosis [33]. These results suggested that the micelles may deliver TP to the target cells and exert their anti-tumor effect.

#### Pharmacokinetic analysis of mPEG-ADH/TP micelles

Table 3 displays the pharmacokinetic variables of unencapsulated TP and mPEG-ADH/TP micelles in rats after intravenous administration, while Fig. 7 depicts the drug concentration time curve of the above dosage forms. In comparison with free TP, mPEG-ADH/TP micelles increased the  $C_{max}$

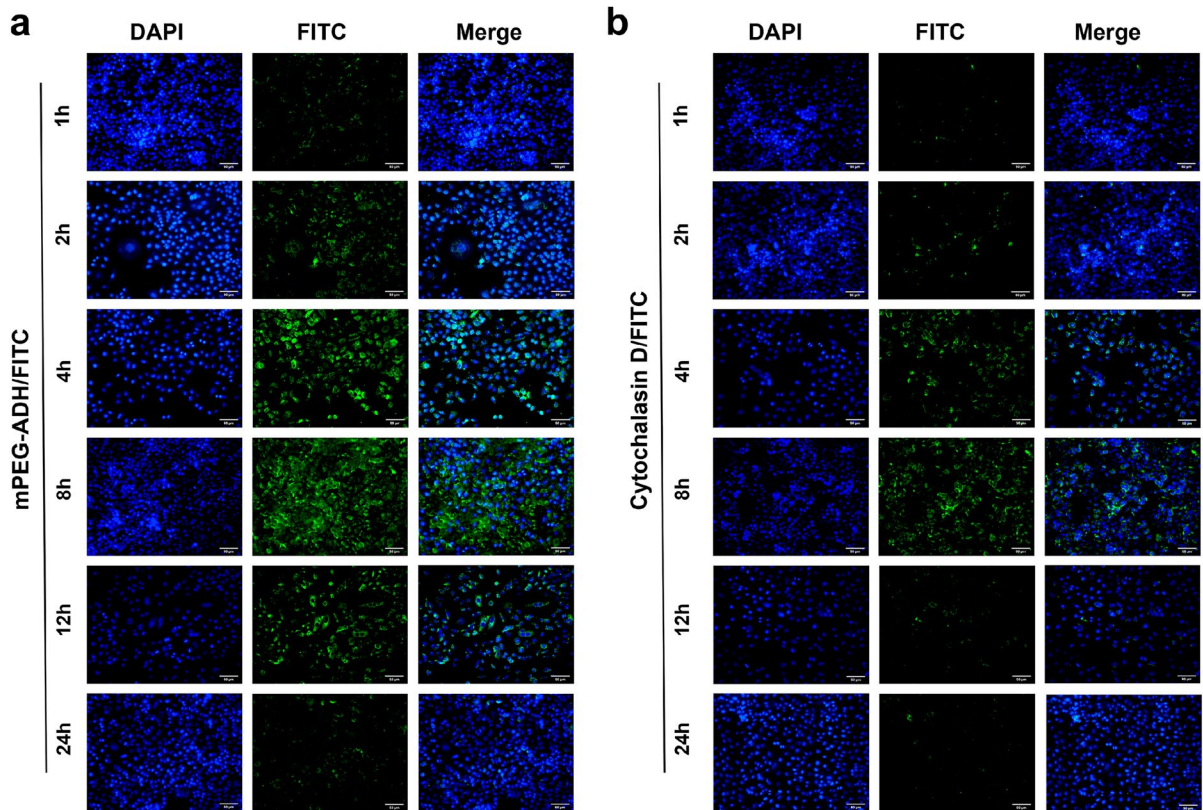


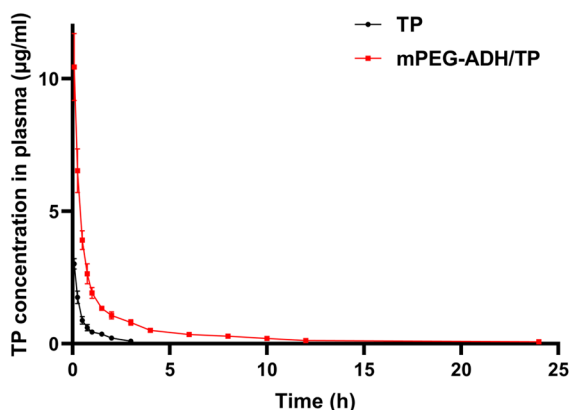
**Fig. 6** In vitro intracellular uptake. Cytofluorogram of A549 cells after incubation with mPEG-ADH/FITC micelles and cytochalasin D/FITC for 1, 2, 4, 8, 12, and 24 h. Blue color

indicated labelled nuclei, green color indicated micelles untaken into cells. Scar bar = 50  $\mu\text{m}$

**Table 3** Plasma pharmacokinetic parameters of methoxy polyethylene glycol- adipic dihydrazide/triptyolide (mPEG-ADH/TP) micelles in rats

Parameters	Unencapsulated TP	mPEG-ADH/TP
$C_{\max}$ ( $\mu\text{g/mL}$ )	$3.02 \pm 0.20$	$10.44 \pm 1.27^{***}$
$T_{\max}$ (h)	0.083	0.083
$T_{1/2}$ (h)	$0.66 \pm 0.05$	$5.42 \pm 0.89^{***}$
$AUC_{0-\infty}$ ( $\mu\text{g/mL} \cdot \text{h}$ )	$1.68 \pm 0.12$	$14.08 \pm 1.60^{***}$
MRT (h)	$2.97 \pm 0.40$	$146.97 \pm 54.93^{***}$

\*\*\* $p < 0.001$ , significant as compared to the free TP group

**Fig. 7** Plasma concentration–time profiles of unencapsulated triptyolide (TP) and methoxy polyethylene glycol- adipic dihydrazide/TP (mPEG-ADH/TP) micelles

dramatically ( $10.44 \pm 1.27 \mu\text{g/mL}$  vs.  $3.02 \pm 0.20 \mu\text{g/mL}$ ,  $p < 0.001$ ). At each point, we observed increased TP concentration in plasma in mPEG-ADH/TP micelles compared to unencapsulated TP. Furthermore, TP elimination from circulation was delayed by mPEG-ADH/TP micelles, which was derived from a substantial lengthy half-life ( $5.42 \pm 0.89$  h vs.  $0.66 \pm 0.05$  h,  $p < 0.001$ ), as well as delayed MRT ( $146.97 \pm 54.93$  h vs.  $2.97 \pm 0.40$  h,  $p < 0.001$ ). More importantly, the AUC values of mPEG-ADH/TP micelles were 8 times that of unencapsulated TP ( $14.08 \pm 1.60 \mu\text{g/mL} \cdot \text{h}$  vs.  $1.68 \pm 0.12 \mu\text{g/mL} \cdot \text{h}$ ,  $p < 0.001$ ).

#### Proliferation inhibition

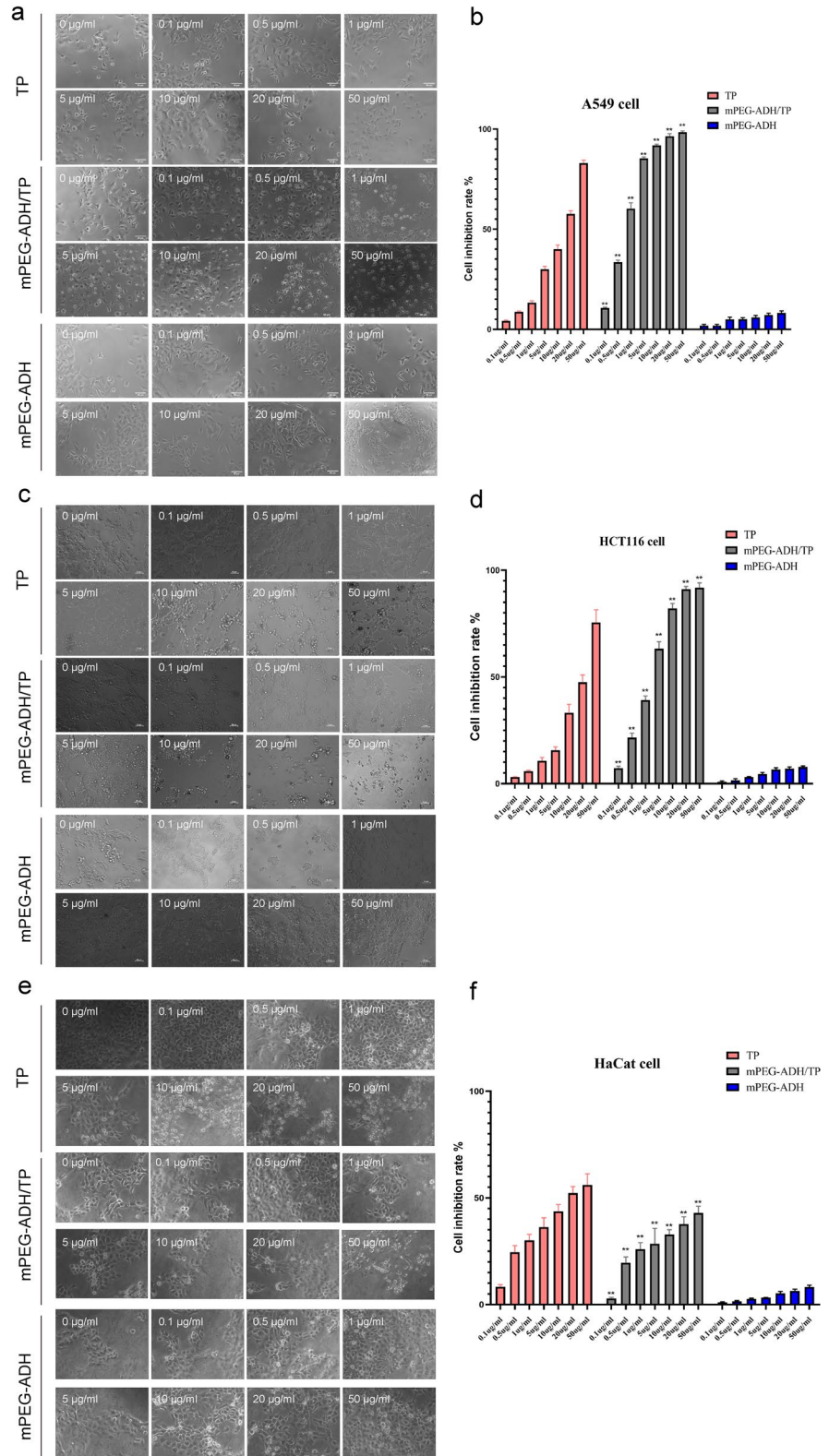
The MTT assay was utilized to evaluate the cytotoxicity of different concentrations of mPEG-ADH/TP micelles and unencapsulated TP on A549 cells.

Within the range 0.1 to 50  $\mu\text{g/mL}$ , the cell inhibition rates of A549 cells with TP and mPEG-ADH/TP micelles increased with an increase in TP concentration. Meanwhile, the mPEG-ADH/TP micelles remarkably suppressed the tumor tissues compared to unencapsulated TP ( $p < 0.05$ ; Fig. 8). We have additionally carried out the cytotoxicity of mPEG-ADH/TP micelles in HCT116 and normal (HaCat) cell lines for comparative analysis, wherein the results showed that mPEG-ADH (all studied concentrations) exhibited an insignificant cytotoxic effect on A459, HCT116, and HaCat cell lines. The mPEG-ADH/TP micelles demonstrated dose-dependent and significant cytotoxic effect on A459 and HCT116 cell line compared to free TP, albeit observation of the reverse in HaCat cell line, wherein the cell inhibition rates were substantially higher (in dose-dependent manner) in free TP-treated cells compared to mPEG-ADH/TP micelles. Cell apoptotic evaluation could affirm the above findings. Thus, we observed similar trends of MTT findings when we determined apoptosis of A549 cells after they have been treated with above dosage forms and control drug. The apoptotic rates increased with increasing TP concentration, and reached a maximum (41.7% cell apoptosis) at 50  $\mu\text{g/mL}$  of mPEG-ADH/TP micelles (Fig. 9). Different concentrations of mPEG-ADH/TP micelles increased cell death compared with the corresponding concentration of free TP, which confirmed that mPEG-ADH/TP micelles possessed excellent therapeutic effect.

#### LD50 calculation and HE staining results of rat liver

The LD50 of TP and mPEG-ADH/TP micelles were 1.474 mg/kg and 2.274 mg/kg, respectively (Fig. 10a). The pharmacokinetic dose used in this study was 1 mg/kg. HE pathological section analysis on the liver of rats in the 1.0 and 2.0 mg/kg groups of TP and mPEG-ADH/TP was performed, and the results showed that the liver of the TP group with different doses showed significant damage, including cell edema, cell membrane damage, cell nucleus destruction, and the presence of blood cells. The liver damage in rats was significantly reduced in the mPEG ADH/TP group at a dose of 1 mg/kg, while the damage was also more pronounced in the mPEG ADH/TP group at a dose of 2 mg/kg (Fig. 10b).

**Fig. 8** Inhibition detection for in vitro evaluation of antitumor activity. Relative cell inhibition of A549 cells (a, b), HCT116 cells (c, d), and HaCat cells (e, f) after 48 h incubation of a series concentration (0, 0.1, 0.5, 1, 5, 10, 20, and 50 µg/mL) of unencapsulated triptolide (TP), methoxy polyethylene glycol- adipic dihydrazide/ TP (mPEG-ADH/TP) micelles, and mPEG-ADH (\*\**p* < 0.05, compared to the unencapsulated TP group)



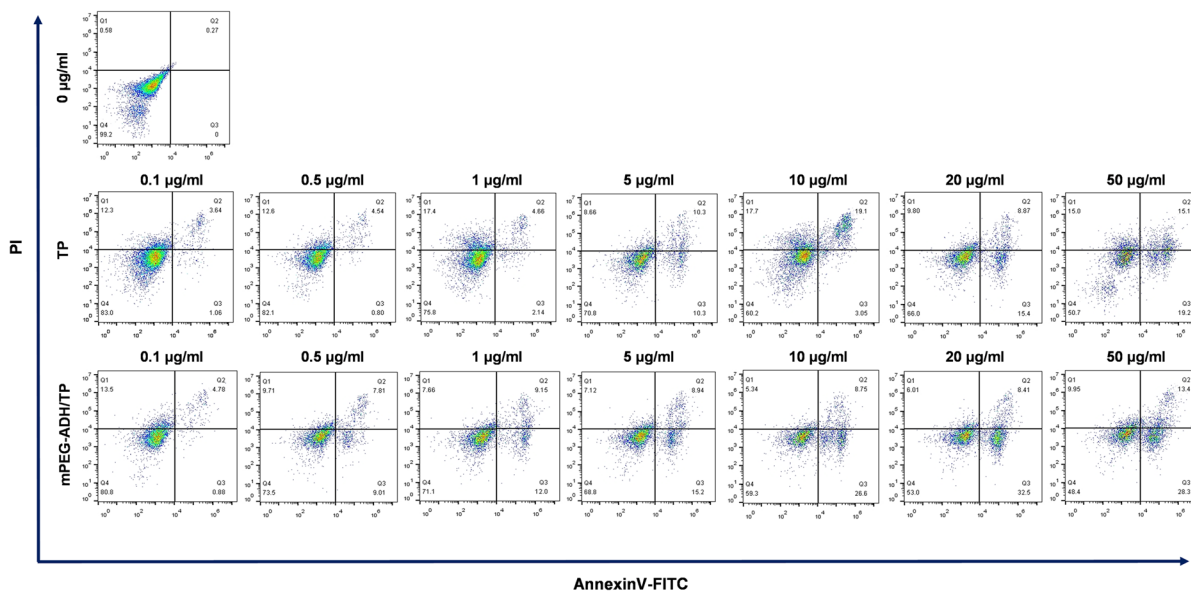


**Fig. 9** Apoptosis analysis for in vitro evaluation of anti-tumor activity. The Annexin-V/PI apoptosis assay of A549 cells after treated with series concentration (0, 0.1, 0.5, 1, 5, 10, 20, and 50 µg/mL) of unencapsulated triptolide (TP) and (TP) and

methoxy polyethylene glycol- adipic dihydrazide/TP (mPEG-ADH/TP) micelles for 48 h measured by flow cytometric analysis

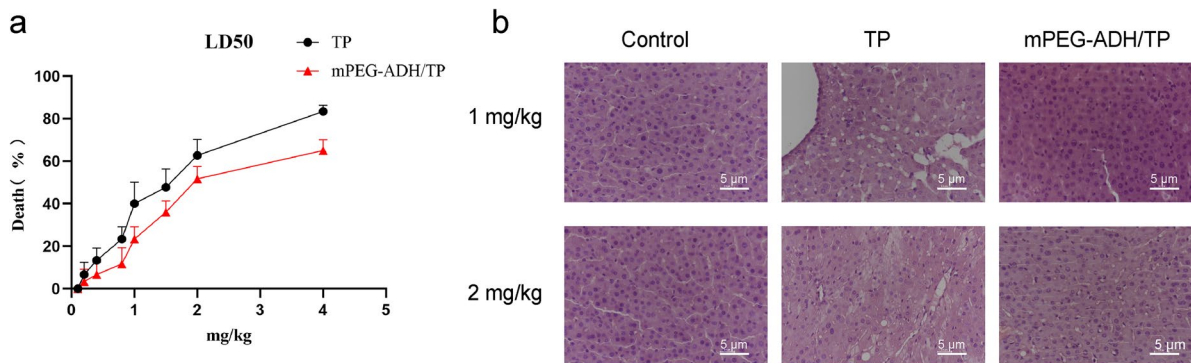


**Fig. 10** LD50 values (a) and HE staining of rat liver (b) after intravenous injection of TP and mPEG-ADH/TP

### Discussion

In this paper, we developed a novel pH-sensitive triptolide-loaded micelle system for enhancing the anti-tumor activity of the diterpenoid epoxide. We synthesized the PEG-ADH copolymer and prepared the TP-loaded micelles by a solvent evaporation method.

We characterized the physicochemical properties, in vitro cytotoxicity, hemolysis, and cellular uptake of the micelles. We also evaluated the in vivo pharmacokinetics, cellular internalization, in vitro anti-tumor efficacy, and toxicity of the micelles.

Our results showed that the micelles had a low CMC, a small and uniform size, a negative surface

charge, and a high drug-loading capacity. These features are desirable for drug delivery systems, as they can improve the solubility, stability, and bioavailability of the encapsulated drug [34, 35]. The micelles also showed low cytotoxicity and hemolysis, indicating their biocompatibility and safety [36, 37]. Moreover, the micelles were rapidly hydrolyzed by esterases, demonstrating their biodegradability and environmental friendliness [38]. The micelles exhibited a pH-sensitive behavior, as they swelled and disintegrated at acidic pH, releasing TP rapidly. This property is advantageous for tumor-targeted drug delivery, as the tumor microenvironment is usually acidic due to the glycolytic metabolism of cancer cells. The pH-sensitive micelles can thus respond to the tumor pH and release the drug on demand, enhancing the therapeutic effect and reducing the side effects [39]. The rapid release of TP under acidic pH has been established in previous works. The release of unencapsulated TP has been found to be burst-like, albeit the release rate being inconsistent among various studies. Existing works suggest that unencapsulated TP achieved complete release (100%) within 2 h at pH 1.2 and pH 7.4 [40, 41]. In contrast, we observed the release rate of TP through the dialysis bags to be over 50% in pH 6.8 and pH 7.4 media but 50% in pH 5.0 solution. Wu et al. observed that the release of free TP across the dialysis bag was rapid (roughly 89%) within 10 h in pH 5.8 and pH 7.4 media [42]. Also, Liu and colleagues discovered the amount of free TP that was released rapidly from the dialysis membrane within 0.5 h was approximately 76.3% in pH 7.4 buffered solution [43]. Besides, Liu and co-authors posited that TP suspension burst-release TP through dialysis membrane within 0.5 h (roughly 70%) before reaching a plateau within 2 h (approximately 80%) [44]. Collectively, the findings of these studies imply inconsistency in the release rates of TP through dialysis membrane, which may potentially be ascribed to several factors including solubility of TP in dissolution media and dialysis membrane molecular weight cutoff [45, 46]. Moreover, the observed rapid release of TP from mPEG-ADH/TP micelles may be ascribable to the favorable interaction between mPEG-ADH and properties of the release medium (especially pH), which can substantially accelerate the release pattern of drug. On the basis of existing literature, we developed this nano-carrier system with a chemical bond that is labile at acidic pH, which is similar to

the acidic microenvironment of tumour. It has been suggested that an aldehyde-specific reagent like ADH can form reversible hydrazone linkages with the carbonyl group of hydrophobic drugs such as TP. In particular, the C18 carbonyl group of TP can form hydrazone bond with ADH. In view of its rapid rate of hydrolysis at acidic pH, hydrazone bond is considered one of the most extensively used pH-sensitive linkages in the applications. Thus, it is used to potentially increase the circulation time of drugs and reduce systemic toxicity.

The micelles were efficiently taken up by hepatocytes and macrophages, which are the main target cells for TP in cancer therapy. The TP exerts its anti-tumor activity by modulating various signaling pathways and inducing apoptosis, autophagy, and immunogenic cell death in cancer cells [47]. The micelles can thus deliver TP to the tumor cells and trigger the desired biological responses. As a colorimetric assay, the MTT technique assesses the metabolic activity of cells, wherein actively metabolizing viable cells convert MTT into a soluble purpled-formazan crystal. On the other hand, the principle of Annexin-V/PI assay is that it detects apoptotic cells with surface phosphatidylserine on their surface and also provides data about the proportion of dead and live cells within the population. The assay also involves fluorescence labeling of the Annexin V, in combination with staining of a nucleus, thus allowing a distinction between early, healthy, and late apoptotic cells via flow cytometric technique. Although the Annexin is considered to be fairly robust when it is used for the detection of suspension-growing cells, it can produce anomalous results owing to potential cellular damage induced by shear forces [48]. It has been suggested that two principal processes may be responsible for the reduction in number of viable cells, namely suppression of cell metabolism and/or actual cell death (cytotoxic effect) or proliferation (cytostatic effect), wherein scientists should discern these from each other [49]. This is the reason why a combination of assays is used to understand the biochemical processes occurring in the cell. The observed discrepancy between the MTT assay and the apoptosis analysis upon treatment of mPEG-ADH/TP micelles at 50 µg/mL to A549 cells (Fig. 10) could stem from various factors intrinsic to the characteristics of the two assays and behavior of the cells under investigation. More importantly, this observed inhibition rate

of mPEG-ADH/TP micelles may be to some extent facilitated through proliferation arrest that does not actually lead to cell death [50]. Xie et al. observed that TP demonstrated anti-proliferative effect in A459 cells, albeit discrepancy in the inhibition ratio determined by MTT assay and apoptotic rate obtained via Annexin-V/PI assay. Also, it is possible that the observed apoptotic rate suggests that mPEG-ADH/TP micelles treatment induced early apoptosis in A459 cells [51].

The micelles improved the pharmacokinetic profile and biodistribution of TP, as they prolonged the blood circulation time and increased the accumulation of TP in the tumor site [52]. The micelles also enhanced the anti-tumor efficacy and reduced the toxicity of TP, as they inhibited the tumor growth, prolonged the survival, and decreased the body weight loss and the liver and kidney damage of the mice. These results indicated that the micelles can overcome the limitations of TP, such as its poor solubility, low bioavailability, and severe toxicity, and improve its therapeutic potential for cancer treatment. Our study suggested that the pH-sensitive and biodegradable micelles are a promising delivery system for TP, as they can enhance its pharmacokinetics, biodistribution, anti-tumor efficacy, and safety. Notwithstanding, not-too-distant future works of our group will comprehensively assess the *in vivo* toxicity and anti-tumor effect of mPEG-ADH/TP micelles, which will enhance the clinical applications of this nanocarrier. In particular, further studies will be needed to explore the molecular mechanisms and immunological aspects of the micelles, to evaluate their long-term safety and toxicity profiles, to compare their performance with other delivery systems for TP, and to validate their clinical efficacy and feasibility in cancer patients. Hopefully, our study will stimulate more research on the development of novel drug delivery systems for TP and other diterpenoid epoxides.

## Conclusions

In summary, we synthesized a pH-sensitive material (mPEG-ADH) with good safety profile successfully. The TP-loaded mPEG-ADH micelles were prepared with small particle size, excellent PDI, and stable property, while the EE (%) was up to 89.87%. Importantly,

the TP in the mPEG-ADH/TP micelles was almost completely released at acidic pH (pH 5.0), while the drug was released slowly and sparingly at physiological pH (pH 7.4). The results suggest the release of TP from mPEG-ADH/TP micelles was sensitive to pH, which could facilitate targeting of the drug into intracellularly low pH endosomes and lysosomes as well as enhance cytotoxicity in cancer tissues. Moreover, mPEG-ADH/TP micelles exhibited excellent proliferation inhibition on tumor cells. Taken together, mPEG-ADH/TP micelles could act as a promising alternative to enhance the efficacy of oncologic treatments.

**Acknowledgements** The authors greatly appreciate all the authors.

**Author contributions** Conceptualization, Zhimeng Lu and Kun Yan; methodology, Zhimeng Lu and Kun Yan; validation, Guiping Yu and Hao Zhang; formal analysis, Chunlei Liu; data curation, Jiapeng Wang; writing—original draft preparation, Zhimeng Lu and Kun Yan; writing—review and editing, Guiping Yu and Hao Zhang. All authors read and approved the final manuscript.

**Funding** This work was supported by the 2022 Jiangsu Graduate Research and Practice Innovation Plan Project (SJCX22\_1283), Jiangsu Provincial Health Commission Health Research Project (M2020076), Wuxi “Double Hundred” Top Talents Project in Medical and Health Care for Middle and Young People (BJ2020104) and Open project of Lung Cancer Sub-bank of Jiangsu Major Diseases Bioresource Sample Bank (SBK202004006).

**Data availability** The datasets used and/or analyzed during the current study are available from the corresponding author on reasonable request.

## Declarations

**Ethics approval** Research experiments conducted in this article with animals were approved by Ethical Committee for laboratory animal experimentation at Jiangsu University in conformity with the rule of thumb governing the use and care of laboratory rodents (UJS-IACUC-2022101505).

**Conflict of interest** The authors declare they have no competing financial interests.

**Open Access** This article is licensed under a Creative Commons Attribution 4.0 International License, which permits use, sharing, adaptation, distribution and reproduction in any medium or format, as long as you give appropriate credit to the original author(s) and the source, provide a link to the Creative Commons licence, and indicate if changes were made. The images or other third party material in this article are included in the article's Creative Commons licence, unless indicated otherwise in a credit line to the material. If material is not

included in the article's Creative Commons licence and your intended use is not permitted by statutory regulation or exceeds the permitted use, you will need to obtain permission directly from the copyright holder. To view a copy of this licence, visit <http://creativecommons.org/licenses/by/4.0/>.

## References

- Law SK-Y, Simmons MP, Techen N, Khan IA, He M-F, Shaw P-C, But PP-H (2011) Molecular molecular analyses of the Chinese herb Leigongteng (*Tripterygium wilfordii* Hook.f.). *Phytochemistry* 72:21–26. <https://doi.org/10.1016/j.phytochem.2010.10.015>
- Wang C, Li CJ, Yang JZ, Ma J, Chen XG, Hou Q, Zhang DM (2013) Anti-inflammatory sesquiterpene derivatives from the leaves of *Tripterygium wilfordii*. *J Nat Prod* 76:85–90. <https://doi.org/10.1021/np300759u>
- Li CJ, Xie FG, Yang JZ, Luo YM, Chen XG, Zhang DM (2012) Two sesquiterpene pyridine alkaloids and a triterpenoid saponin from the root barks of *Tripterygium hypoglauca*. *J Asian Nat Prod Res* 14:973–980. <https://doi.org/10.1080/10286020.2012.729049>
- Guo X, Xue M, Li CJ, Yang W, Wang SS, Ma ZJ, Zhang XN, Wang XY, Zhao R, Chang BC, Chen LM (2016) Protective effects of triptolide on TLR4 mediated auto-immune and inflammatory response induced myocardial fibrosis in diabetic cardiomyopathy. *J Ethnopharmacol* 193:333–344. <https://doi.org/10.1016/j.jep.2016.08.029>
- Chugh R, Sangwan V, Patil SP, Dudeja V, Dawra RK, Banerjee S, Schumacher RJ, Blazar BR, Georg GI, Vickers SM, Saluja AK (2012) A preclinical evaluation of minnelide as a therapeutic agent against pancreatic cancer. *Sci Transl Med* 4:156ra139. <https://doi.org/10.1126/scitranslmed.3004334>
- Jiang L, Shestov AA, Swain P, Yang C, Parker SJ, Wang QA, Terada LS, Adams ND, McCabe MT, Pietrak B, Schmidt S, Metallo CM, Dranka BP, Schwartz B, DeBerardinis RJ (2016) Reductive carboxylation supports redox homeostasis during anchorage-independent growth. *Nature* 532:255–258. <https://doi.org/10.1038/nature17393>
- Jiang C, Fang X, Zhang H, Wang X, Li M, Jiang W, Tian F, Zhu L, Bian Z (2017) Triptolide inhibits the growth of osteosarcoma by regulating microRNA-181a via targeting PTEN gene in vivo and vitro. *Tumour Biol* 39:1010428317697556. <https://doi.org/10.1177/1010428317697556>
- Long C, Guo W, Zhou H, Wang J, Wang H, Sun X (2016) Triptolide decreases expression of latency-associated nuclear antigen 1 and reduces viral titers in Kaposi's sarcoma-associated and herpesvirus-related primary effusion lymphoma cells. *Int J Oncol* 48:1519–1530. <https://doi.org/10.3892/ijo.2016.3353>
- Zhao J, Xie C, Mu X, Krausz KW, Patel DP, Shi X, Gao X, Wang Q, Gonzalez FJ (2018) Metabolic alterations in triptolide-induced acute hepatotoxicity. *Biomed Chromatogr* 32:e4299. <https://doi.org/10.1002/bmc.4299>
- Wang X, Zhao F, Lv ZM, Shi WQ, Zhang LY, Yan M (2016) Triptolide disrupts the actin-based sertoli-germ cells adherens junctions by inhibiting Rho GTPases expression. *Toxicol Appl Pharmacol* 310:32–40. <https://doi.org/10.1016/j.taap.2016.08.017>
- Shi J, Ren Y, Ma J, Luo X, Li J, Wu Y, Gu H, Fu C, Cao Z, Zhang J (2021) Novel CD44-targeting and pH/redox-dual-stimuli-responsive core-shell nanoparticles loading triptolide combats breast cancer growth and lung metastasis. *J Nanobiotechnol* 19:188. <https://doi.org/10.1186/s12951-021-00934-0>
- Yalikong A, Li XQ, Zhou PH, Qi ZP, Li B, Cai SL, Zhong YS (2021) A triptolide loaded HER2-targeted nano-drug delivery system significantly suppressed the proliferation of HER2-positive and BRAF mutant colon cancer. *Intern J Nanomed* 16:2323–2335. <https://doi.org/10.2147/ijn.S287732>
- Wu Y, Li J, Zhong X, Shi J, Cheng Y, He C, Li J, Zou L, Fu C, Chen M, Zhang J, Gao H (2022) A pH-sensitive supramolecular nanosystem with chlorin e6 and triptolide co-delivery for chemo-photodynamic combination therapy. *Asian J Pharm Sci* 17:206–218. <https://doi.org/10.1016/j.ajps.2021.12.003>
- Zhu D, Zhang Q, Chen Y, Xie M, Li J, Yao S, Li M, Lou Z, Cai Y, Sun X (2022) Mechanochemical preparation of triptolide-loaded self-micelle solid dispersion with enhanced oral bioavailability and improved anti-tumor activity. *Drug Deliv* 29:1398–1408. <https://doi.org/10.1080/10717544.2022.2069879>
- Wang Y, Liu X, Wang X, Zheng W, Zhang J, Shi F, Liu J (2018) Redox-responsive self-assembly PEG nanoparticle enhanced triptolide for efficient antitumor treatment. *Sci Rep* 8:12968. <https://doi.org/10.1038/s41598-018-29692-0>
- Liu C, Jiang T-t, Yuan Z-x, Lu Y (2020) Self-assembled casein nanoparticles loading triptolide for the enhancement of oral bioavailability. *Nat Prod Commun* 15. <https://doi.org/10.1177/1934578x20948352>
- Liu H, Shen M, Zhao D, Ru D, Duan Y, Ding C, Li H (2019) The effect of triptolide-loaded exosomes on the proliferation and apoptosis of human ovarian cancer SKOV3 cells. *Biomed Res Int* 2019:2595801. <https://doi.org/10.1155/2019/2595801>
- Haley B, Frenkel E (2008) Nanoparticles for drug delivery in cancer treatment. *Urol Oncol* 26:57–64. <https://doi.org/10.1016/j.urolonc.2007.03.015>
- Zhou Q, Zhang L, Yang T, Wu H (2018) Stimuli-responsive polymeric micelles for drug delivery and cancer therapy. *Intern J Nanomed* 13:2921–2942. <https://doi.org/10.2147/ijn.S158696>
- Rapoport N (2007) Physical stimuli-responsive polymeric micelles for anti-cancer drug delivery. *Prog Polym Sci* 32:962–990. <https://doi.org/10.1016/j.progpolymsci.2007.05.009>
- Torchilin VP (2001) Targeted polymeric micelles for delivery of poorly soluble drugs. *Cell Mol Life Sci* 61:2549–2559. <https://doi.org/10.1007/s00018-004-4153-5>
- Torchilin V (2011) Tumor delivery of macromolecular drugs based on the EPR effect. *Adv Drug Deliv Rev* 63:131–135. <https://doi.org/10.1016/j.addr.2010.03.011>
- Wang Z, Deng X, Ding J, Zhou W, Zheng X, Tang G (2018) Mechanisms of drug release in pH-sensitive micelles for tumour targeted drug delivery system: a review. *Int J Pharm* 535:253–260. <https://doi.org/10.1016/j.ijpharm.2017.11.003>



24. Qiao Y, Wan J, Zhou L, Ma W, Yang Y, Luo W, Yu Z, Wang H (2019) Stimuli-responsive nanotherapeutics for precision drug delivery and cancer therapy. Wiley Interdiscip Rev Nanomed Nanobiotechnol 11:e1527. <https://doi.org/10.1002/wnan.1527>
25. Yang Y, Chen Q, Lin J, Cai Z, Liao G, Wang K, Bai L, Zhao P, Yu Z (2019) Recent advance in polymer based microspheric systems for controlled protein and peptide delivery. Curr Med Chem 26:2285–2296. <https://doi.org/10.2174/0929867326666190409130207>
26. Huang P, Wang G, Su Y, Zhou Y, Huang W, Zhang R, Yan D (2019) Stimuli-responsive nanodrug self-assembled from amphiphilic drug-inhibitor conjugate for overcoming multidrug resistance in cancer treatment. Theranostics 9:5755–5768. <https://doi.org/10.7150/thno.36163>
27. Li Z, Yin Y (2019) Stimuli-responsive optical nanomaterials. Adv Mater 31:e1807061. <https://doi.org/10.1002/adma.201807061>
28. Sun Y, Zhan A, Zhou S, Kuang X, Shen H, Liu H, Xu Y (2019) A novel mitochondria-targeting tetrapeptide for subcellular delivery of nanoparticles. Chin Chem Lett 30:1435–1439. <https://doi.org/10.1016/j.ccllet.2019.05.001>
29. Qiu H, Gao Y, Boott CE, Gould OEC, Harniman RL, Miles MJ, Webb SED, Winnik MA, Manners I (2016) Uniform patchy and hollow rectangular platelet micelles from crystallizable polymer blends. Science 352:697–701. <https://doi.org/10.1126/science.aad9521>
30. Shi F, Du M, Wang Q, Adu-Frimpong M, Li C, Zhang X, Ji H, Toreniyazov E, Cao X, Wang Q, Xu X (2023). Isoliquiritigenin containing PH sensitive micelles for enhanced anti-colitis activity. J Pharm Sci 28:S0022-3549(23)00383-0. <https://doi.org/10.1016/j.xphs.2023.09.020>
31. Wang S, Guo Q, Xu R, Lin P, Deng G, Xia X (2023) Combination of ferroptosis and pyroptosis dual induction by triptolide nano-MOFs for immunotherapy of Melanoma. J Nanobiotechnol 21(1):383. <https://doi.org/10.1186/s12951-023-02146-0>
32. He L, Sayers EJ, Watson P, Jones AT (2018). Contrasting roles for actin in the cellular uptake of cell penetrating peptide conjugates. Sci Rep 8:7318. <https://doi.org/10.1038/s41598-018-25600-8>
33. Lin HP, Singla B, Ghoshal P, Faulkner JL, Cherian-Shaw M, O'Connor PM, She JX, Belin de Chantemele EJ, Csányi G (2018). Identification of novel macropinocytosis inhibitors using a rational screen of Food and Drug Administration-approved drugs. Br J Pharmacol 175(18):3640–3655. <https://doi.org/10.1111/bph.14429>
34. Lu Y, Zhang E, Yang J, Cao Z (2018) Strategies to improve micelle stability for drug delivery. Nano Res 11:4985–4998. <https://doi.org/10.1007/s12274-018-2152-3>
35. Ayala V, Herrera AP, Latorre-Esteves M, Torres-Lugo M, Rinaldi C (2013) Effect of surface charge on the colloidal stability and in vitro uptake of carboxymethyl dextran-coated iron oxide nanoparticles. J Nanopart Res 15:1874. <https://doi.org/10.1007/s11051-013-1874-0>
36. Zhang CX, Cheng Y, Liu DZ, Liu M, Cui H, Zhang BL, Mei QB, Zhou SY (2019) Mitochondria-targeted cyclosporin a delivery system to treat myocardial ischemia reperfusion injury of rats. J Nanobiotechnol 17:18. <https://doi.org/10.1186/s12951-019-0451-9>
37. Hocking KM, Evans BC, Komalavilas P, Cheung-Flynn J, Duvall CL, Brophy CM (2019) Nanotechnology enabled modulation of signaling pathways affects physiologic responses in intact vascular tissue. Tissue Eng Part A 25:416–426. <https://doi.org/10.1089/ten.TEA.2018.0169>
38. Danaei M, Kalantari M, Raji M, Samareh Fekri H, Saber R, Asnani GP, Mortazavi SM, Mozafari MR, Rasti B, Taheriazam A (2018) Probing nanoliposomes using single particle analytical techniques: effect of excipients, solvents, phase transition and zeta potential. Heliyon 4:e01088. <https://doi.org/10.1016/j.heliyon.2018.e01088>
39. Zhou B, Li X, Tang H, Miao Z, Feng H, Li Y (2011) Total synthesis of novel D-ring-modified triptolide analogues: structure-cytotoxic activity relationship studies on the D-ring of triptolide. Org Biomol Chem 9:3176–3179. <https://doi.org/10.1039/c0ob01239d>
40. Zhang C, Gu C, Peng F, Liu W, Wan J, Xu H, Lam CW, Yang X (2013) Preparation and optimization of triptolide-loaded solid lipid nanoparticles for oral delivery with reduced gastric irritation. Molecules 18(11):13340–13356. <https://doi.org/10.3390/molecules181113340>
41. Li M, Wang G, Yan Y, Jiang M, Wang Z, Zhang Z, Wu X, Zeng H (2022) Triptolide and l-ascorbate palmitate co-loaded micelles for combination therapy of rheumatoid arthritis and side effect attenuation. Drug Delivery 29(1):2751–2758. <https://doi.org/10.1080/10717544.2022.2115162>
42. Wu Y, Li J, Zhong X, Shi J, Cheng Y, He C, Li J, Zou L, Fu C, Chen M, Zhang J, Gao H (2022) A pH-sensitive supramolecular nanosystem with chlorin e6 and triptolide co-delivery for chemo-photodynamic combination therapy. Asian J Pharm Sci 17(2):206–218. <https://doi.org/10.1016/j.ajps.2021.12.003>
43. Liu C, Jiang T, Yuan Z, Lu Y (2020). Self-assembled casein nanoparticles loading triptolide for the enhancement of oral bioavailability. Nat Prod Commun 15(8):1934578X2094835. <https://doi.org/10.1177/1934578X20948352>
44. Jia L, Nie XQ, Ji HM, Yuan ZX, Li RS (2021). Multiple-coated PLGA nanoparticles loading triptolide attenuate injury of a cellular model of Alzheimer's disease. Biomed Res Int 2021:8825640. <https://doi.org/10.1155/2021/8825640>
45. Shen J, Burgess DJ (2013) In vitro dissolution testing strategies for nanoparticulate drug delivery systems: recent developments and challenges. Drug Deliv Transl Res 3(5):409–415. <https://doi.org/10.1007/s13346-013-0129-z>
46. D'Souza S (2014) A review of in vitro drug release test methods for nano-sized dosage forms. Adv Pharm 2014:1–12. <https://doi.org/10.1155/2014/304757>
47. Mussi SV, Sawant R, Perche F, Oliveira MC, Azevedo RB, Ferreira LA, Torchilin VP (2014) Novel nanostructured lipid carrier co-loaded with doxorubicin and docosahexaenoic acid demonstrates enhanced in vitro activity and overcomes drug resistance in MCF-7/Adr cells. Pharm Res 31:1882–1892. <https://doi.org/10.1007/s11095-013-1290-2>
48. Henslee EA, Torcal Serrano RM, Labeed FH, Jabr RI, Fry CH, Hughes MP, Hoettges KF (2016) Accurate quantification of apoptosis progression and toxicity using a dielectrophoretic approach. Analyst 141:6408. <https://doi.org/10.1039/c6an01596d>

49. Sazonova EV, Chesnokov MS, Zhivotovsky B, Kopeina GS (2022) Drug toxicity assessment: cell proliferation versus cell death. *Cell Death Discov* 8:417. <https://doi.org/10.1038/s41420-022-01207-x>
50. Xie CQ, Zhou P, Zuo J, Li X, Chen Y, Chen JW (2016) Triptolide exerts pro-apoptotic and cell cycle arrest activity on drug-resistant human lung cancer A549/Taxol cells via modulation of MAPK and PI3K/Akt signaling pathways. *Oncol Lett* 12(5):3586–3590. <https://doi.org/10.3892/ol.2016.5099>
51. Liu S, Zhang J, Zhang X, Zhang H, Li X, Zhang S (2016) Triptolide induces cell apoptosis in human stomach cancer cell via caspase 3-dependent cascade pathway. *Trop J Pharm Res* 15(9):1853. <https://doi.org/10.4314/tjpr.v15i9.6>
52. Luo W, Wen G, Yang L, Tang J, Wang J, Wang J, Zhang S, Zhang L, Ma F, Xiao L, Wang Y, Li Y (2017) Dual-targeted and pH-sensitive doxorubicin prodrug-microbubble complex with ultrasound for tumor treatment. *Theranostics* 7:452–465. <https://doi.org/10.7150/thno.16677>

**Publisher's Note** Springer Nature remains neutral with regard to jurisdictional claims in published maps and institutional affiliations.